Enhanced power conversion efficiency in InGaN-based solar cells *via* graded composition multiple quantum wells

Yu-Lin Tsai,[1] Sheng-Wen Wang,[1] Jhih-Kai Huang,[1] Lung-Hsing Hsu,[2] Ching-Hsueh Chiu,[1] Po-Tsung Lee,[1] Peichen Yu,[1] Chien-Chung Lin,[2,*] and Hao-Chung Kuo,[1,3]

[1]*Department of Photonics and Institute of Electro-Optical Engineering, National Chiao Tung University, Hsinchu 30010, Taiwan*

[2] *Institute of Photonic System, College of Photonics, National Chiao-Tung University, Tainan 71150, Taiwan*

[3]*hckuo@faculty.nctu.edu.tw*

[*]*chienchunglin@faculty.nctu.edu.tw*

Abstract: This work demonstrates the enhanced power conversion efficiency (PCE) in InGaN/GaN multiple quantum well (MQWs) solar cells with gradually decreasing indium composition in quantum wells (GQWs) toward p-GaN as absorber. The GQW can improve the fill factor from 42% to 62% and enhance the short current density from 0.8 mA/cm^2 to 0.92 mA/cm^2, as compares to the typical MQW solar cells. As a result, the PCE is boosted from 0.63% to 1.11% under AM1.5G illumination. Based on simulation and experimental results, the enhanced PCE can be attributed to the improved carrier collection in GQW caused by the reduction of potential barriers and piezoelectric polarization induced fields near the p-GaN layer. The presented concept paves a way toward highly efficient InGaN-based solar cells and other GaN-related MQW devices.

OCIS codes: (040.5350) Photovoltaic; (350.6050) Solar energy; (040.4200) Multiple quantum well.

References and links

1. O. Jani, I. Ferguson, C. Honsberg, and S. Kurtz, "Design and characterization of GaN/ InGaN solar cells," Appl. Phys. Lett. **91**(13), 132117 (2007).
2. J. Wu, W. Walukiewicz, K. M. Yu, W. Shan, J. W. Ager III, E. E. Haller, H. Lu, W. J. Schaff, W. K. Metzger, and S. Kurtz, "Superior radiation resistance of $In_{1-x}Ga_xN$ alloys: Full-solar-spectrum photovoltaic material system," J. Appl. Phys. **94**(10), 6477 (2003).
3. A. G. Bhuiyan, K. Sugita, A. Hashimoto, and A. Yamamoto, "InGaN Solar Cells: Present state of the art and important challenges," IEEE J. Photovolt. **2**(3), 276–293 (2012).
4. H. W. Wang, P. Yu, Y. R. Wu, H. C. Kuo, E. Y. Chang, and S. H. Lin, "Projected efficiency of polarization-matched p-$In_xGa_{1-x}N$/i-$In_yGa_{1-y}N$/n-GaN double heterojunction solar cells," IEEE J. Photovolt. **3**(3), 985–990 (2013).
5. C. C. Yang, C. H. Jang, J. K. Sheu, M. L. Lee, S. J. Tu, F. W. Huang, Y. H. Yeh, and W. C. Lai, "Characteristics of InGaN-based concentrator solar cells operating under 150X solar concentration," Opt. Express **19**(S4 Suppl 4), A695–A700 (2011).
6. W. E. McMahon, C. T. Lin, J. S. Ward, J. F. Geisz, M. W. Wanlass, J. J. Carapella, W. Olavarr'ıa, M. Young, M. A. Steiner, R. M. France, A. E. Kibbler, A. Duda, J. M. Olson, E. E. Perl, D. J. Friedman, and J. E. Bowers, "Metal pillar interconnection topology for bonded two-terminal multijunction III–V solar cells," IEEE J. Photovolt. **3**(2), 868–872 (2013).
7. D. H. Lien, Y. H. Hsiao, S. G. Yang, M. L. Tsai, T. C. Wei, S. C. Lee, and J. H. He, "Harsh photovoltaics using InGaN/GaN multiple quantum well schemes," Nano Energy **11**, 104–109 (2015).
8. A. Luque and A. Martí, "Increasing the efficiency of ideal solar cells by photon induced transitions at intermediate levels," Phys. Rev. Lett. **78**(26), 5014–5017 (1997).
9. M. Leyer, J. Stellmach, C. Meissner, M. Pristovsek, and M. Kneissl, "The critical thickness of InGaN on (0 0 0 1) GaN," J. Cryst. Growth **310**(23), 4913–4915 (2008).
10. X. Zheng, R. H. Horng, D. S. Wuu, M. T. Chu, W. Y. Liao, M. H. Wu, R. M. Lin, and Y. C. Lu, "High-quality InGaN/GaN heterojunctions and their photovoltaic effects," Appl. Phys. Lett. **93**(26), 261108 (2008).

#240328 Received 4 May 2015; revised 9 Sep 2015; accepted 15 Sep 2015; published 30 Sep 2015

11. Y. L. Tsai, C. C. Lin, H. V. Han, C. K. Chang, H. C. Chen, K. J. Chen, W. C. Lai, J. K. Sheu, F. I. Lai, P. Yu, and H. C. Kuo, "Improving efficiency of InGaN/GaN multiple quantum well solar cells using CdS quantum dots and distributed Bragg reflectors," Sol. Energy Mater. Sol. Cells **117**, 531–536 (2013).
12. Y. A. Chang, F. M. Chen, Y. L. Tsai, C. W. Chang, K. J. Chen, S. R. Li, T. C. Lu, H. C. Kuo, Y. K. Kuo, P. Yu, C. C. Lin, and L. W. Tu, "Fabrication and characterization of back-side illuminated InGaN/GaN solar cells with periodic via-holes etching and Bragg mirror processes," Opt. Express **22**(S5), A1334–A1342 (2014).
13. J. K. Sheu, F. B. Chen, S. H. Wu, M. L. Lee, P. C. Chen, and Y. H. Yeh, "Vertical InGaN-based green-band solar cells operating under high solar concentration up to 300 suns," Opt. Express **22**(S5), A1222–A1228 (2014).
14. R. M. Farrell, C. J. Neufeld, S. C. Cruz, J. R. Lang, M. Iza, S. Keller, S. Nakamura, S. P. DenBaars, U. K. Mishra, and J. S. Speck, "High quantum efficiency InGaN/GaN multiple quantum well solar cells with spectral response extending out to 520 nm," Appl. Phys. Lett. **98**(20), 201107 (2011).
15. S. Valdueza-Felip, A. Mukhtarova, L. Grenet, C. Bougerol, C. Durand, J. Eymery, and E. Monroy, "Improved conversion efficiency of as-grown InGaN/GaN quantum-well solar cells for hybrid integration," Appl. Phys. Express **7**(3), 032301 (2014).
16. A. Alemu, J. A. H. Coaquira, and A. Freundlich, "Dependence of device performance on carrier escape sequence in multi-quantum-well p-i-n solar cells," J. Appl. Phys. **99**(8), 084506 (2006).
17. H. Fujii, K. Toprasertpong, Y. Wang, K. Watanabe, M. Sugiyama, and Y. Nakano, "100-period, 1.23-eV bandgap InGaAs/GaAsP quantum wells for high-efficiency GaAs solar cells: toward current-matched Ge-based tandem cells," Prog. Photovolt. Res. Appl. **22**(7), 784–795 (2014).
18. P. T. Barletta, E. Acar Berkman, B. F. Moody, N. A. El-Masry, A. M. Emara, M. J. Reed, and S. M. Bedair, "Development of green, yellow, and amber light emitting diodes using InGaN multiple quantum well structures," Appl. Phys. Lett. **90**(15), 151109 (2007).
19. Z. Deng, Y. Jiang, Z. Ma, W. Wang, H. Jia, J. Zhou, and H. Chen, "A novel wavelength-adjusting method in InGaN-based light-emitting diodes," Sci. Rep. **3**, 3389 (2013).
20. K. Y. Lai, G. J. Lin, Y. R. Wu, M. L. Tsai, and J. H. He, "Efficiency dip observed with InGaN-based multiple quantum well solar cells," Opt. Express **22**(S7), A1753–A1760 (2014).
21. S. F. Chichibu, A. Uedono, T. Onuma, B. A. Haskell, A. Chakraborty, T. Koyama, P. T. Fini, S. Keller, S. P. Denbaars, J. S. Speck, U. K. Mishra, S. Nakamura, S. Yamaguchi, S. Kamiyama, H. Amano, I. Akasaki, J. Han, and T. Sota, "Origin of defect-insensitive emission probability in In-containing (Al,In,Ga)N alloy semiconductors," Nat. Mater. **5**(10), 810–816 (2006).
22. Y. C. Yao, M. T. Tsai, C. Y. Huang, T. Y. Lin, J. K. Sheu, and Y. J. Lee, "Efficient collection of photogenerated carriers by inserting double tunnel junctions in III-nitride p-i-n solar cells," Appl. Phys. Lett. **103**(19), 193503 (2013).
23. J. R. Lang, N. G. Young, R. M. Farrell, Y. R. Wu, and J. S. Speck, "Carrier escape mechanism dependence on barrier thickness and temperature in InGaN quantum well solar cells," Appl. Phys. Lett. **101**(18), 181105 (2012).
24. J. Yang, D. G. Zhao, D. S. Jiang, P. Chen, Z. S. Liu, L. C. Le, X. G. He, X. J. Li, and H. Yang, "Effects of quantum well number on spectral response of InGaN/GaN multiple quantum well solar cells," Phys. Status Solidi A **211**(9), 2157–2160 (2014).
25. S. B. Choi, J. P. Shim, D. M. Kim, H. I. Jeong, Y. D. Jho, Y. H. Song, and D. S. Lee, "Effect of indium composition on carrier escape in InGaN/GaN multiple quantum well solar cells," Appl. Phys. Lett. **103**(3), 033901 (2013).
26. Y.-H. Ra, R. Navamathavan, J.-H. Park, and C.-R. Lee, "Radial growth behavior and characteristics of m-plane $In_{0.16}Ga_{0.84}N$/GaN MQW nanowires by MOCVD," CrystEngComm **15**(10), 1874 (2013).
27. J. Piprek, *Semiconductor Optoelectronic Devices* (Academic, 2003).
28. C. J. Neufeld, S. C. Cruz, R. M. Farrell, M. Iza, J. R. Lang, S. Keller, S. Nakamura, S. P. DenBaars, J. S. Speck, and U. K. Mishra, "Effect of doping and polarization on carrier collection in InGaN quantum well solar cells," Appl. Phys. Lett. **98**(24), 243507 (2011).
29. APSYS, Crosslight Software Inc, Vancouver, BC, Canada, 2012.
30. Y. K. Kuo, Y. A. Chang, H. W. Lin, J. Y. Chang, S. H. Yen, F. M. Chen, and Y. H. Chen, "Advantages of InGaN solar cells with p-doped and high-Al-content superlattice AlGaN barriers," IEEE Photonics Technol. Lett. **25**(1), 85–87 (2013).
31. S. L. Chuang and C. S. Chang, "K•p method for strained wurtzite semiconductors," Phys. Rev. B **54**(4), 2491–2504 (1996).
32. S. L. Chuang and C. S. Chang, "A band-structure model of strained quantum-well wurtzite semiconductors," Semicond. Sci. Technol. **12**(3), 252–263 (1997).

1. Introduction

Due to the beneficial photovoltaic properties, including a direct bandgap with energies from 0.7 eV (InN) to 3.4 eV (GaN), a high absorption coefficient (of the order of 10^5 cm^{-1}), high carrier mobility, InGaN-based solar cells becomes potential candidate to realize full-solar-spectrum utilization [1–5]. Recently, the combination of InGaN-based solar cells and conventional GaAs-based multi-junction solar cells by using bonding techniques was proposed to push the efficiencies of concentrated photovoltaics beyond 50% [6]. Moreover,

#240328 Received 4 May 2015; revised 9 Sep 2015; accepted 15 Sep 2015; published 30 Sep 2015

the InGaN-based solar cells has also been demonstrated as a harsh environment-sustainable photovoltaic devices, which can be operated in high-temperature and high-energy radiation conditions [7]. Based on these advantages, InGaN-based solar cells is one of the candidates for highly efficient self-powered harsh devices.

To have a thick InGaN absorber with a relatively high indium composition is one of the critical challenges in InGaN-based solar cells. In general, the critical thickness of InGaN decreases rapidly with the increase of indium composition [8]. Once the thickness of InGaN exceeds this critical value, many defects could be formed as recombination centers, increasing the consumption rate of photo-generated electron-hole pairs, and thus degrading the photovoltaic performance [9]. Therefore, the power conversion efficiency (PCE) of InGaN-based heterojunction solar cells is still low [10].

To maintain the quality of the deposited InGaN eiplayer with high indium content, an alternative structure of multiple quantum wells (MQWs) was used to develop high efficiency InGaN-based solar cells [11–13]. Previous studies have demonstrated that the most of high PCE were acquired from the structure of n-GaN/MQW/p-GaN [14,15]. However, the carrier collection in MQW solar cells can be seriously affected by carrier confinement effect. Therefore, the carrier collection in MQW solar cells is an important factor to determine the PCE [16]. In contrast with the GaAs-based MQW solar cells [17], GaN-based MQW solar cells grown on c-plane sapphire substrate suffer from the spontaneous and strain induced piezoelectric polarizations, which become more significant as the indium composition of MQWs increase [18–20]. Unfortunately, the direction of polarization field is opposite to the built-in field direction of the p-n junction, which reduces of the overall electric field in the MQWs [21]. This leads to the reduction of the built-in field and thus degrading the carrier collection capability and PCE of solar cells [22]. From the previous studies, the PCE in n-GaN/MQW/p-GaN solar cells depends on various parameters of MQW structures, including the thickness of quantum barriers [23], the periods of MQWs [24] and the indium composition of MQWs [25]. However, the approach to improve PCE in InGaN/GaN MQW solar cells through the MQW band-diagram engineering is scarcely reported.

In this study, InGaN/GaN MQW solar cells with gradually decreasing indium composition in quantum wells (graded quantum well, GQWs) toward p-GaN as the absorber is demonstrated with an improved PCE. Due to the reduced polarization field and potential barrier near the p-GaN layer brought by GQW design, the short circuit current density (J_{SC}) was increased from 0.8 mA/cm^2 to 0.92 mA/cm^2 and the PCE was boosted from 0.63% to 1.11% under AM1.5G illumination, as compared to the typical MQW solar cell. The improvements of carrier collection and PCE in InGaN/GaN GQW solar cell were demonstrated by both simulating and measuring their band diagram, current density-voltage (J-V) and bias dependence external quantum efficiency (EQE). The presented concept paves a way for highly efficient InGaN-based solar cells and other MQW devices.

2. Experiments

Figure 1(a) shows the schematic diagram of InGaN/GaN typical MQW and GQW solar cell. The solar cells were grown by metal-organic chemical vapor deposition (MOCVD) on a c-plane sapphire substrate. The typical MQW solar cell is comprised of a 30nm-thick, low-temperature GaN nucleation layer and a 2μm-thick undoped GaN layer on sapphire substrate, 14-period $In_{0.135}Ga_{0.865}N$/GaN (3 nm/5 nm) undoped MQWs sandwiched by a 2μm-thick Si-doped n-GaN layer and a 100nm-thick Mg-doped p-GaN layer. For GQW solar cell, the GQW absorber is comprised of 14-period $In_xGa_{1-x}N$/GaN (3 nm/5 nm) and the indium composition of quantum wells is gradually decreased from 16% to 10% towards p-GaN. The indium composition distributions in typical MQW and GQW are as shown in Fig. 1(b). The indium compositions of GQW solar cell is designed to match the optical absorption of typical MQW solar cell so that the difference in photovoltaic characteristic won't be brought by different optical absorption. After the growth, a regular process procedure was applied to

#240328 Received 4 May 2015; revised 9 Sep 2015; accepted 15 Sep 2015; published 30 Sep 2015

fabricate InGaN-based solar cells. A 110nm-thick indium-tin-oxide (ITO) was deposited on to p-GaN by a sputtering system. The device was then defined into a 2 × 2 mm^2 mesa by an inductively coupled plasma reactive ion etching (ICP-RIE) system. Finally, Cr/Pt/Au (50/50/190 nm) was deposited by electron-beam evaporation, which serves as the p-GaN and the n-GaN contact metal.

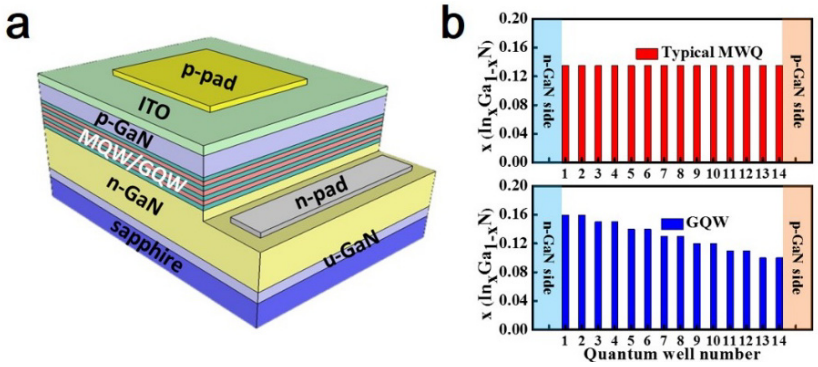

Fig. 1. (a) Schematic plots of the fabricated InGaN/GaN typical MQW and GQW solar cell. (b) The indium composition distributions in typical MQW and GQW absorber.

3. Results and discussion

To investigate the indium composition of MQW, the photoluminescence (PL) spectra at room temperature of the typical MQW cell and GQW cell were measured as shown in Fig. 2(a) and 2(b), respectively. The full width at half maximum (FWHM) of PL spectrum of GQW is wider than that of the typical MQW which indicates the existence of multiple indium composition in GQW solar cell. To estimate the indium composition, the Gaussian function was used to fit the PL spectra. As shown in Fig. 2(a) and 2(b), the number of Gaussian function required for fitting the PL spectra of typical MQW cell and GQW cell are two and seven, respectively. The fitted peak wavelengths of typical MQW cell are 432nm and 447nm. The second peak (447nm) of typical MQW solar cell in Fig. 2(a) can be attributed to the indium fluctuation or phase separation [26]. For the GQW cell, the fit peak wavelengths are 413nm, 420nm, 426nm, 431nm, 437nm, 442nm and 451nm. Each peak wavelength can be linked to one corresponding indium composition. The relation between bandgap energy (eV) and mole fraction of the alloy element (x<0.2) at room temperature has been reported in previous studies [27]:

$$E_g = 0.7x + 0.34(1-x) - 1.43x(1-x) \quad (1)$$

Through this formula, the corresponding indium composition of QWs can be obtained. The corresponding indium composition of typical MQW cell are x = 0.135 and 0.16, and x = 0.1, 0.113, 0.124, 0.135, 0.144, 0.152 and 0.168 for GQW cell, respectively. The broadened PL with multiple peaks wrapped in the spectrum can be viewed as the successful growth of GQW absorbers.

#240328 Received 4 May 2015; revised 9 Sep 2015; accepted 15 Sep 2015; published 30 Sep 2015

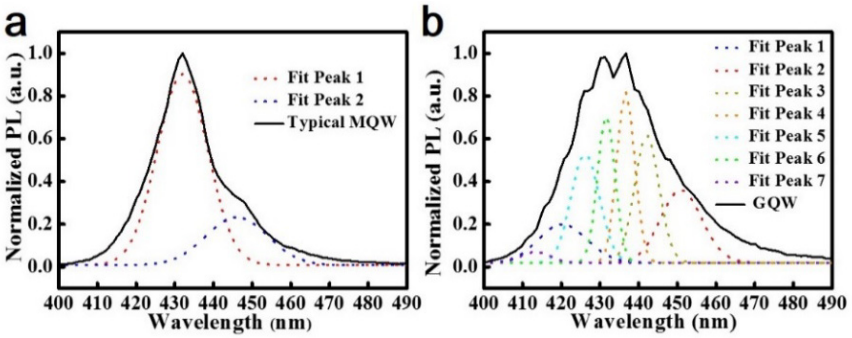

Fig. 2. Room temperature PL emission spectra of (a) typical MQW and (b) GQW solar cell.

Figure 3(a) and 3(b) plots the dark current-voltage curves and current density-voltage curves under AM1.5G illumination conditions of the typical MQW and GQW solar cell, respectively, and the detailed parameters are listed in Table 1. The devices were operated under a 1000 W Class A solar simulator with AM1.5G spectrum. The temperature was maintained at 25°C during the measurements using an automatic temperature control system. In Fig. 3(a), the two dark current curves are similar and this indicates that the leakage current due to the threading dislocation density are at the same level. In addition, from the result in Fig. 3(b), the reversed saturation current density (J_S) of these two samples are approximately the same, and this phenomenon demonstrates that the maximal photo-generated carriers are the same for typical MQW and GQW solar cell. Therefore, the difference in photovoltaic characteristics will not be brought by different crystal quality and optical absorption, and the effect of GQW can be clearly observed. As shown in Fig. 3(b), the fill factor (F.F.) increases from 42% of typical MQW solar cell to 62% of GQW solar cell, and the short-circuit current density (J_{SC}) increases from 0.8 mA/cm^2 of typical MQW solar cell to 0.92 mA/cm^2 of GQW solar cells. As compared with the illuminated J-V curve of these two samples, the GQW cell has 1 curve break as a normal solar cells and the typical MQW solar cell has 2 curve breaks. This phenomenon indicates that the photovoltaic characteristic of typical MQW solar cell is seriously affected by the strain induced electrical field and insufficiently doped GaN than GQW solar cell [28]. By introducing the GQW absorber, the PCE was boosted from 0.63% to 1.11% corresponding to a 74.6% enhancement, as compared to the typical MQW solar cell.

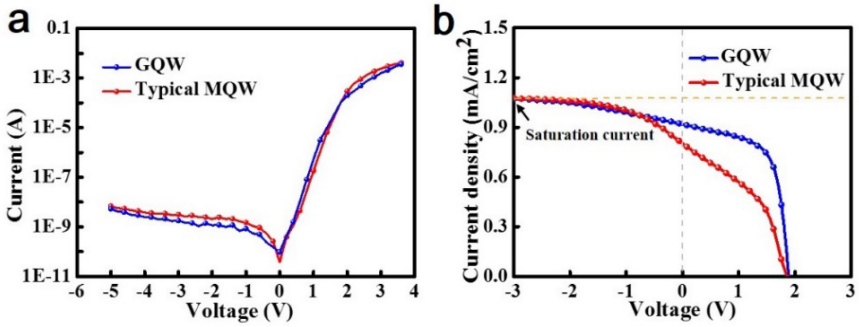

Fig. 3. (a) Current-voltage curve under dark situation. (b) Current density-voltage (J-V) curve of typical MQW and GQW solar cell under AM1.5G illumination condition.

#240328 Received 4 May 2015; revised 9 Sep 2015; accepted 15 Sep 2015; published 30 Sep 2015

Table 1. Current-voltage characteristics of typical MQW and GQW solar cell under AM1.5G illumination condition.

	V_{oc} (V)	J_{sc} (mA/cm^2)	Fill factor (%)	Efficiency (%)
Typical MQW	1.87	0.8	42	0.63
GQW	1.88	0.92	64	1.11

The external quantum efficiency (EQE) is an important characteristic for revealing the solar cells performance. Figure 4(a) plots the EQE of the typical MQW and GQW solar cell at zero bias. The GQW cell exhibits an overall EQE enhancement at wavelengths from 300 to 425 nm. To elucidate further the carrier collection in different excitation wavelength, Fig. 4(b) presents the enhancement ratio of GQW solar cell relative to the typical MQW solar cell, here we define the enhancement ratio as Eq. (2)

$$Enhancement\ ratio = EQE_{GQW} / EQE_{typical\ MQW} \tag{2}$$

It should not be neglected that a significantly peak in EQE is observed at wavelengths in the range of 300-320 nm; this peak can be attributed to both the enhanced built-in electrical field and the reduced potential barriers in GQW near the p-GaN layer. Most of electron-hole pairs generated by high energy photons in solar cells are located in quantum wells which is close to the p-GaN. Therefore, the collection of such electron-hole pairs can be dramatically affected by the design of MQW. However, the GQW not only improves the carrier collection of higher energy-photon-generated electron-hole pairs (300-320 nm) but also the lower energy-photon-generated electron-hole pairs (320-420 nm). To further investigate the carrier collection of typical MQW and GQW solar cell, the EQE of these two kinds of solar cell are measured as a function of applied reverse bias from 0 V to −1.5 V as shown in Fig. 4(c) and 4(d). As the device is reverse biased, the EQE spectral response is improved in broadband, indicating that the applied reverse bias increases the net electrical field across the InGaN quantum well region and promotes the carrier collection in MQW absorber. As the reverse bias is applied on the device with poor carrier collection capability, the carrier collection of the device would be effectively improved. From the results in Fig. 4(c) and 4(d), the enhancement change in EQE of typical MQW solar cell is stronger than that of in GQW solar cell as the applied reverse bias increased, which indicates the carrier collection in GQW is better than that in typical MQW.

#240328 Received 4 May 2015; revised 9 Sep 2015; accepted 15 Sep 2015; published 30 Sep 2015

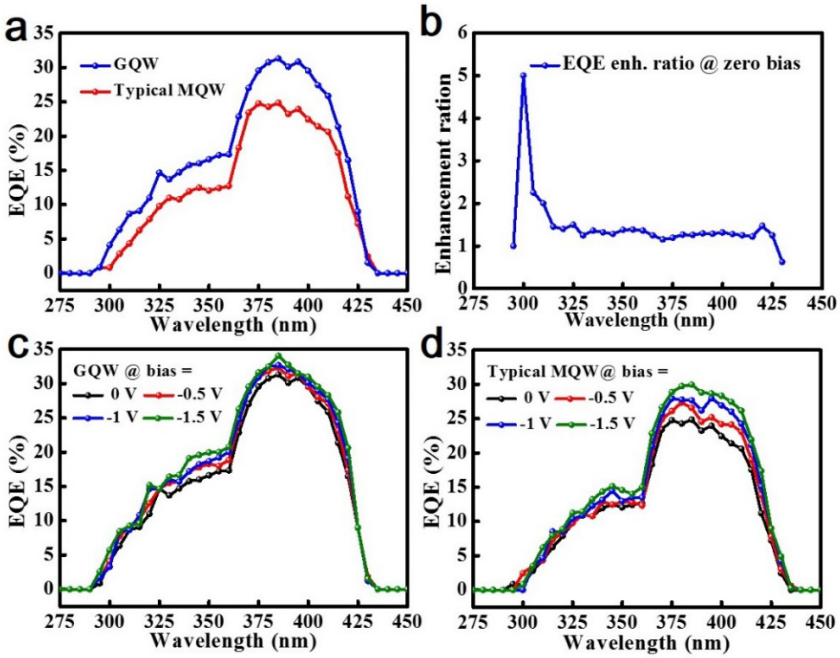

Fig. 4. (a) The external quantum efficiency (EQE) of typical MQW and GQW solar cell and (b) the corresponding enhancement ratio in EQE. Bias dependence EQE of (c) GQW and (d) typical MQW solar cell under the bias voltage of 0V, −0.5V, −1V and −1.5V.

To further evaluate these two designs numerically, the widely-used APSYS software is adapted in our study [29,30]. The simulator employs 6 × 6 k•p model developed for the strained wurtzite semiconductor by Chuang and Chang [31,32] to calculate the energy band structures, and the interactions between photons and carriers including absorptions, generations, recombinations, and transportations are taken into calculations.

The simulated band diagram of the typical MQW cell and the GQW cell with zero bias under the AM 1.5G illumination are shown in Fig. 5(a) and the detailed band diagram are shown in Fig. 5(b) and 5(c). For the GQW cell, the larger bandgap of quantum wells provide better band alignment to p-GaN layer, enhancing the net electric field in MQW absorber to collect the photo-generated carrier, especially at the region close to the p-GaN. Moreover, the lattice match between quantum well and barrier of GQW structure is better around the p-GaN layer and thus the sheet polarized charge and the electric field against carrier-collection are both reduced. As shown in Fig. 5(b) and 5(c), the potential barriers close to the p-GaN layer of GQW cell are much smaller than that of in typical MQW cell for both conduction and valence band, and the reduction of potential barriers promotes the carrier collection probability in the MQW absorber. On the other hand, the higher valance band potential barriers close to the n-GaN layer of GQW solar cell obstruct the photo-generated holes to n-GaN layer, and reduce the recombination rate at n-GaN layer. Figure 5(d) shows the photo-generated hole distribution in these two types of solar cell. The photo-generated hole concentration at p-GaN of GQW cell is higher than that of in typical MQW cell. This result indicates that more carrier are collected. Therefore, the enhanced PCE can be acquired in InGaN/GaN GQW solar cell.

#240328 Received 4 May 2015; revised 9 Sep 2015; accepted 15 Sep 2015; published 30 Sep 2015

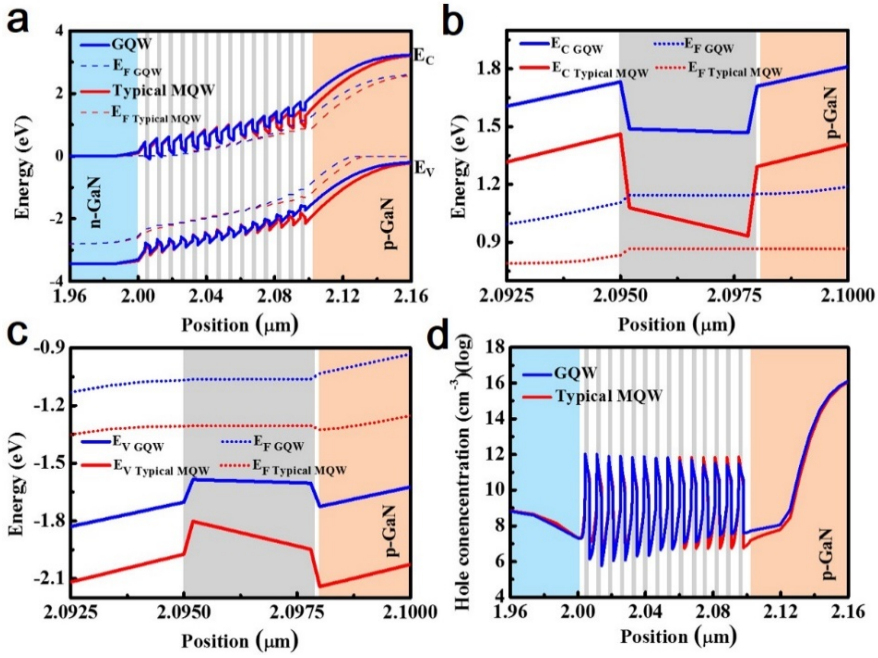

Fig. 5. (a) Simulated band diagram and (b) detailed band diagram in final quantum well at p-GaN interface for conduction band and (c) valence band of GQW and typical MQW solar cell. (d) Hole concentration distribution of GQW and typical MQW solar cell.

4. Conclusion

In conclusion, the enhanced power conversion efficiency (PCE) in InGaN/GaN MQW solar cells was demonstrated with gradually decreasing indium composition in quantum wells (GQWs) toward p-GaN. The GQW absorber reduced not only the polarized charge induced field but also the potential barriers close to the p-GaN layer, to boost the carrier collection of InGaN/GaN MQW solar cells. By introducing the GQW design, the fill factor was improved from 42% of typical MQW solar cell to 62% of GQW solar cell. As a result, the PCE was boosted from 0.63% to 1.1% corresponding to a 74.6% enhancement. The GQW design provides a promising scheme for highly efficient InGaN/GaN MQW solar cells and should be beneficial to other types of GaN-related quantum well devices.

Acknowledgment

This work was supported by the Ministry of Science and Technology of Taiwan, under Grants MOST 104-2628-E-009-013-MY3, NSC-102-3113-P-009-007-CC2, NSC-102-2221-E-009-131-MY3 and NSC-102-2112-M-018-004-MY3.

#240328 Received 4 May 2015; revised 9 Sep 2015; accepted 15 Sep 2015; published 30 Sep 2015